

Unusual signatures of the ferromagnetic transition in the heavy Fermion compound $\text{UMn}_2\text{Al}_{20}$

C. H. Wang^{1,2,3}, J. M. Lawrence¹, E. D. Bauer², K. Kothapalli⁴, J. S. Gardner^{5,6}, F. Ronning², K. Gofryk², J. D. Thompson², H. Nakotte⁴, F. Trouw²

¹University of California, Irvine, California 92697

²Los Alamos National Laboratory, Los Alamos, NM 87545

³Neutron Scattering Science Division, Oak Ridge National Laboratory, Oak Ridge, TN, 37831

⁴Department of Physics, New Mexico State University, Las Cruces, 88003

⁵NCNR, National Institute of Standards and Technology, Gaithersburg, MD 20899-6102

⁶Indiana University, Bloomington, Indiana 47408

(Dated: August 8, 2018)

Magnetic susceptibility results for single crystals of the new cubic compounds $\text{UT}_2\text{Al}_{20}$ (T=Mn, V, and Mo) are reported. Magnetization, specific heat, resistivity, and neutron diffraction results for a single crystal and neutron diffraction and inelastic spectra for a powder sample are reported for $\text{UMn}_2\text{Al}_{20}$. For T = V and Mo, temperature independent Pauli paramagnetism is observed. For $\text{UMn}_2\text{Al}_{20}$, a ferromagnetic transition is observed in the magnetic susceptibility at $T_c = 20$ K. The specific heat anomaly at T_c is very weak while no anomaly in the resistivity is seen at T_c . We discuss two possible origins for this behavior of $\text{UMn}_2\text{Al}_{20}$: moderately small moment itinerant ferromagnetism, or induced local moment ferromagnetism.

Introduction $\text{UMn}_2\text{Al}_{20}$, $\text{UV}_2\text{Al}_{20}$ and $\text{UMo}_2\text{Al}_{20}$ are members of a new family of lanthanide and actinide compounds RT_2M_{20} (R=Ce, Yb, Gd, U; T=transition metal; M=Zn and Al)¹⁻⁷. These compounds crystallize in the $\text{CeCr}_2\text{Al}_{20}$ type cubic structure (F d -3 m) and display interesting features such as heavy fermion or intermediate valence behavior⁴⁻⁷. In this structure, every f -atom is surrounded by 16 zinc atoms in a nearly spherical array of cubic site symmetry, which leads to small crystal field splittings. Because the R-atom content is less than 5% of the total number of atoms, and the shortest f/f spacing is ~ 6 Å, these compounds are valuable for studies close to the impurity limit but in ordered systems.

We have recently reported on the behavior of the heavy Fermion paramagnets $\text{UCo}_2\text{Zn}_{20}$ ^{5,8} and $\text{URu}_2\text{Zn}_{20}$ ⁸ as well as of $\text{UIr}_2\text{Zn}_{20}$ ⁶, which exhibits weak itinerant ferromagnetism. In this report we present the magnetic susceptibility of $\text{UMn}_2\text{Al}_{20}$, $\text{UV}_2\text{Al}_{20}$ and $\text{UMo}_2\text{Al}_{20}$, and the specific heat, resistivity, magnetization, and neutron scattering spectra for $\text{UMn}_2\text{Al}_{20}$. For $\text{UV}_2\text{Al}_{20}$ and $\text{UMo}_2\text{Al}_{20}$, Pauli paramagnetism is observed. For $\text{UMn}_2\text{Al}_{20}$, the magnetic susceptibility shows a ferromagnetic phase transition at 20 K where the anomaly in the specific heat is weak and no anomaly is observed in the resistivity. The neutron diffraction profiles of both polycrystal and single crystal samples show no obvious extra contribution from the ferromagnetism below the transition temperature. The inelastic neutron scattering spectra of a polycrystal sample exhibit no obvious magnetic excitations in the energy transfer range of 5 to 50 meV. We discuss two possibilities to explain the magnetic behavior in $\text{UMn}_2\text{Al}_{20}$: heavy Fermion ferromagnetism of itinerant $5f$ electrons or induced ferromagnetism arising from a low energy singlet-triplet crystal field excitation of localized $5f$ electrons.

Experiment Single crystals were grown in Al flux with an elemental starting ratio U:T:Al=1:2:50. Elemental

purities were 99.9% for the (depleted) U, 99.99% for the Mn and 99.9999% for the Al. The crucible was sealed under vacuum in a quartz tube and was heated to 1050°C quickly in order to avoid the reaction between Al and the quartz tube. After holding at 1050°C for 4 h, it was cooled at a rate 5°C/h to 700°C. At this point the excess Al flux was removed by using a centrifuge. The magnetization was measured in a commercial superconducting quantum interference device (SQUID) magnetometer. The specific heat measurements were performed in a commercial physical properties measurement system (PPMS). The electrical resistivity was also measured in the PPMS using the four wire method. The powder neutron diffraction experiment was performed on the high resolution diffractometer (BT-1) at the NIST Center for Neutron Research (NCNR); the sample was a powder ground from single crystals. The single crystal neutron diffraction experiment was performed on the single crystal diffractometer (SCD) at the Lujan Center, LANSCE, at Los Alamos National Laboratory. The inelastic neutron scattering experiments were performed on a 35 gram powder sample using the high resolution chopper spectrometer (Pharos) at the Lujan Center.

Results and Discussion The samples were determined to be single phase within the resolution of the x-Ray, neutron powder, and neutron single crystal diffraction experiments. Refinements of the single crystal and powder sample diffraction patterns imply full occupancy of the atom sites. The results of the refinement are shown in table I. The magnetic susceptibility $\chi(T)$ of $\text{UMn}_2\text{Al}_{20}$ is shown in the inset of Fig. 1(a). A dramatic enhancement at low temperature is observed, indicating a ferromagnetic transition at $T_c \approx 20$ K. Due to the small coercive field (9 Oe, see below), the zero field cooling and field cooling data is almost the same when the measured field is 0.1 T. Due to the relatively small magnetic moment of the uranium ($0.89 \mu_B$, see below) and the small frac-

TABLE I: Structural parameters of $\text{UMn}_2\text{Al}_{20}$ at room temperature from SCD and at 100 K from BT-1. Error in the last digit are in the parentheses.

space group	$Fd\bar{3}m$	no. 227	$a^{SCD}=14.326(6)$	$[a^{BT1}=14.3190(2)]$	$\chi_{SCD}^2=1.984$	$\chi_{BT1}^2=7.053$
Atoms	Position	$x^{SCD}[x^{BT1}]$	$y^{SCD}[y^{BT1}]$	$z^{SCD}[z^{BT1}]$	occupancy	$\text{Uiso}^{SCD}(\times 10^2)$
U	8a	1/8	1/8	1/8	1	2.34
Mn	16d	1/2	1/2	1/2	1	3.15
Al1	16c	0	0	0	1	2.98
Al2	48f	0.4893(4)[0.4913(4)]	1/8	1/8	1	3.56
Al3	96g	0.0589(4)[0.0590(1)]	0.0589(4)[0.0590(1)]	0.3258(4)[0.3259(1)]	1	2.92
		$R(F^2)^{SCD}=4.76\%$	$R_w(F^2)^{SCD}=16.88\%$	$R_p^{BT1}=14.29\%$	$R_{wp}^{BT1}=17.38\%$	

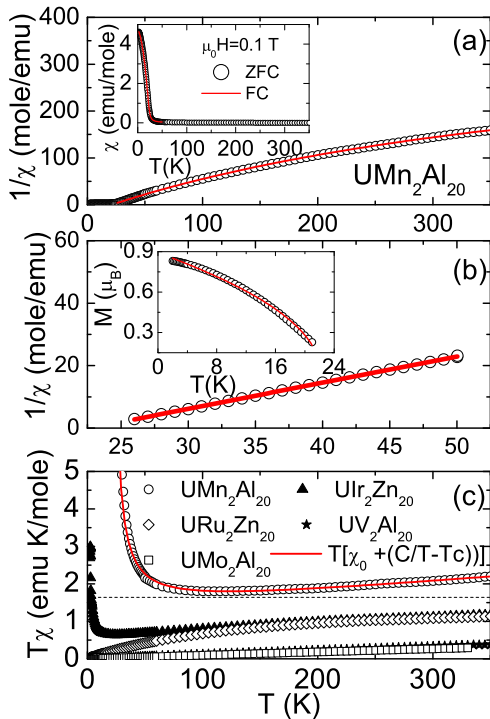


FIG. 1: (a) Inverse magnetic susceptibility $1/\chi(T)$ for $\text{UMn}_2\text{Al}_{20}$. The line represents the modified Curie-Weiss fit $\chi(T) = C/(T - \theta) + \chi_0$ with parameters given in the text. Inset: $\chi(T)$. Open circle is zero-field cooling curve and solid line is the field-cooling curve. (b) Mean field fits for $1/\chi$ in temperature range of 25 K to 50 K (main panel) and for $M(T)$ below the ferromagnetic transition temperature (inset) with parameters given in the text. (c) $T\chi$ vs. T for $\text{UMn}_2\text{Al}_{20}$, $\text{UV}_2\text{Al}_{20}$, $\text{UMo}_2\text{Al}_{20}$, $\text{URu}_2\text{Zn}_{20}$ (data from Ref.⁸) and $\text{UIr}_2\text{Zn}_{20}$ (data from Ref.⁶). The dashed line is the Curie constant for $5f^3$ free ion.

tion of uranium atoms in the unit cell (less than 5%), the neutron diffraction results on both the powder and the single crystal samples did not display any obvious extra intensity at temperatures below the transition temperature that would correspond to ferromagnetic ordering.

The inverse magnetic susceptibility $1/\chi(T)$ of

$\text{UMn}_2\text{Al}_{20}$ is shown in Fig. 1(a). A fit of the inverse susceptibility to the formula $\chi(T) = C/(T - \theta) + \chi_0$ for temperatures above T_c gives $\theta=21.2$ K, $\chi_0=0.00253$ emu/mole, and $C=1.23$ emu K/mole. This value of Curie constant, which is reduced relative the free ion f^2 or f^3 Hund's Rule value 1.6 emu K/mole, is typical of itinerant uranium compounds. The inverse susceptibility $1/\chi(T)$ in the low temperature range (25 K-50 K) is shown in Fig. 1(b). The fit to the form $\chi(T) = C/(T - T_c)^\gamma$ in this temperature range yields $T_c=22.7$ K, $C=1.17$ emu K/mole, and $\gamma = 0.99$, which is essentially the mean field critical exponent ($\gamma=1$). The magnetization $M(T)$ for $T < T_c$ is shown in the inset of Fig. 1(b). The fit to the formula $M = M_0(T_c - T)^\beta$ yields $M_0=0.89 \mu_B$, $T_c=22.1$ K and $\beta=0.49$ which is again the mean field theory exponent ($\beta=0.5$).

The effective moment $T\chi$ versus temperature is compared for several compounds UT_2M_{20} ($T=\text{Mn, Ir, Ru, V}$ and Mo ; $M=\text{Al}$ and Zn) in Fig. 1(c). The dashed line represents the Curie constant for the Hund's Rule coupled $5f^2$ or $5f^3$ free ion. The linear behavior of $T\chi$ for $\text{UV}_2\text{Al}_{20}$ and $\text{UMo}_2\text{Al}_{20}$ indicates that the magnetic susceptibilities for these two compounds are essentially temperature independent; the values 0.0011 emu/mole for $\text{UV}_2\text{Al}_{20}$ and 0.00087 emu/mole for $\text{UMo}_2\text{Al}_{20}$ are typical of uranium based Pauli paramagnets. Both the heavy Fermion compound $\text{URu}_2\text{Zn}_{20}$ and the weak itinerant ferromagnet $\text{UIr}_2\text{Zn}_{20}$ ⁶ exhibit similar behavior at high temperature with $T\chi$ of order 1.2 emu K/mole, similar to the Curie constant observed for $\text{UMn}_2\text{Al}_{20}$ in Figs. 1(a) and (b). For both $\text{UIr}_2\text{Zn}_{20}$ and $\text{UMn}_2\text{Al}_{20}$, the upturn in $T\chi$ at low temperatures corresponds to the onset of ferromagnetic fluctuations, which occur already for $T > T_c$. Given that the formula $\chi(T) = C/(T - \theta) + \chi_0$ fits the data for $\text{UMn}_2\text{Al}_{20}$ above T_c , and that the Curie constant in this fit is smaller than the free ion value, the fact that $T\chi$ is larger than the free ion value for $T > 100$ K clearly arises from the presence of the large constant term $\chi_0 \sim 0.0025$ emu/mole. A possible explanation for this rather large constant contribution is that the susceptibility of the manganese atoms is enhanced. T-independent susceptibilities of this order of magnitude occur, for example, for Mn atoms in alloys of the en-

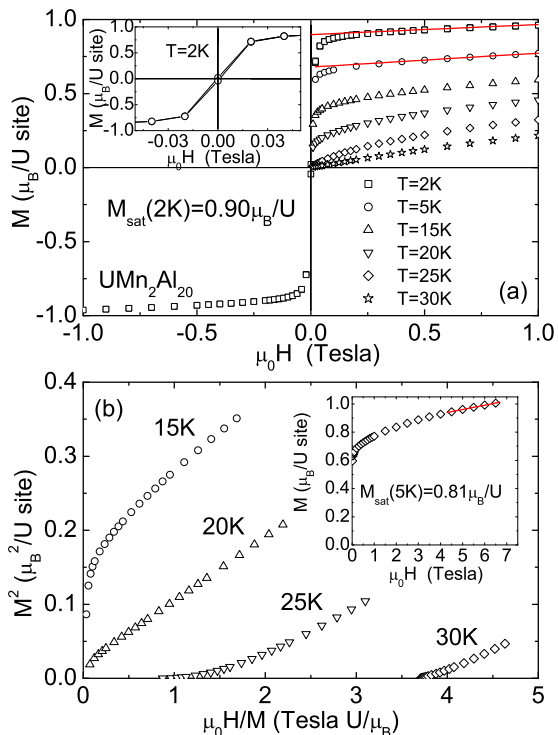


FIG. 2: (a) Magnetization of $\text{UMn}_2\text{Al}_{20}$ at 2 K, 5 K, 15 K, 20 K, 25 K and 30 K. The extrapolations of the solid lines give the saturation magnetization. Inset shows the hysteresis loop at 2 K. (b) Arrott plots for several temperature. Inset shows the magnetization at 5 K at larger fields.

hanced Pauli paramagnet YMn_2 ⁹.

The isothermal magnetization results at various temperature of $\text{UMn}_2\text{Al}_{20}$ are displayed in Fig. 2(a). The full hysteresis loop at 2 K is shown on a zoomed scale in the inset. Both the coercive field and the remnant magnetization are very small with $H_c \sim 9$ Oe and $M_R \sim 0.03 \mu_B$. A linear fit to the magnetization data at 2 K below 1 tesla gives a value $M_{sat}(2\text{K}) = 0.90 \mu_B$ for the saturation magnetization which is essentially the same as the value $M_0 = 0.89 \mu_B$ derived from the mean field fit of Fig. 1(b), inset. A similar extrapolation performed on the 5 K magnetization data below 1 tesla yields $M_{sat}(5\text{K}) = 0.68 \mu_B$ while the value extrapolated from high field (4.5 T to 6.5 T) is $M_{sat}(5\text{K}) = 0.81 \mu_B$. We note that these values are much smaller than the values expected for the $J = 4$ ($5f^2$, $3.58 \mu_B$) or $J = 9/2$ ($5f^3$, $3.62 \mu_B$) free ions. An Arrott plot¹⁰ is displayed in Fig. 2(b); it clearly shows that the Curie temperature T_c is 20-21 K.

The specific heat measurements on $\text{UMn}_2\text{Al}_{20}$ and the nonmagnetic counterpart $\text{ThV}_2\text{Al}_{20}$ are shown in Fig. 3(a). There is no obvious anomaly in the as-measured data of $\text{UMn}_2\text{Al}_{20}$ near T_c . In the inset, a fit to the form $\gamma T + \beta T^3$ yields a linear coefficient 0.3 J/mole K^2 and a Debye temperature $\theta_D = 337 \text{ K}$. The magnetic contribution to the specific heat C_{mag} is obtained by subtracting the lattice contribution which is equated to the specific

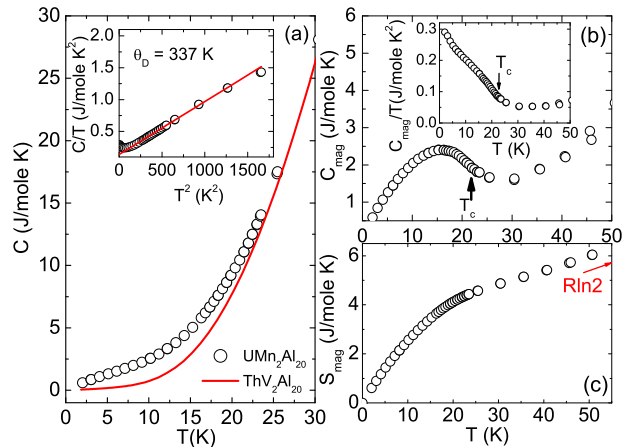


FIG. 3: (a) Specific heat of $\text{UMn}_2\text{Al}_{20}$ and $\text{ThV}_2\text{Al}_{20}$. The inset shows C/T vs. T^2 ; the solid line is a linear fit in the temperature range of 15 K to 40 K. (b) Magnetic contribution to the specific heat. The inset is C_{mag}/T vs. temperature. (c) Magnetic entropy associated with C_{mag} .

heat of the nonmagnetic counterpart $\text{ThV}_2\text{Al}_{20}$. Both C_{mag} and C_{mag}/T are shown in Fig. 3(b). The data for C_{mag} shows a broad peak near 16 K which corresponds to a small anomaly (a curvature change) in C_{mag}/T at the same temperature. The entropy associated with the magnetic specific heat is shown in Fig. 3(c), giving a value for the magnetic entropy of $R\ln 2$ at 46 K and showing a curvature change near T_c .

The resistivity $\rho(T)$ of $\text{UMn}_2\text{Al}_{20}$ is shown in Fig. 4. The resistivity decreases with the decreasing temperature down to 10 K, below which it is a constant. There is no anomaly at 20 K associated with the ferromagnetic transition. We also display the temperature differential curve $d\rho(T)/dT$ in the inset (a) to enhance the possibility of observing a tiny anomaly in $\rho(T)$. There is still no obvious anomaly. We combine a Bloch-Grüneisen resistivity ρ_{BG} together with a parallel resistor ρ_P to fit $\rho(T)$ as:

$$\rho(T)^{-1} = \rho_P^{-1} + (\rho_0 + \rho_{BG})^{-1}$$

where ρ_0 is the residual resistivity. The solid line represents the best fit to the data. The fit gives $\theta_D = 320 \text{ K}$, close to the value θ_D obtained from the specific heat, $\rho_0 = 61.7 \mu\Omega \text{ cm}$, and $\rho_P = 112.8 \mu\Omega \text{ cm}$. This form of resistivity and the magnitude of ρ_P is characteristic of many transition metal and actinide compounds, where the parallel resistivity gives rise to a saturation of the resistivity at a value where the mean free path is comparable to the lattice spacing. Recent theory¹¹ indicates that this saturation happens when the electron phonon interaction destroys lattice periodicity and momentum conservation at elevated temperatures. For $\text{UMn}_2\text{Al}_{20}$, the point of the fit is that the resistivity arises primarily from the electron-phonon interaction, with little indication of magnetic scattering.

The most interesting property of this compound is

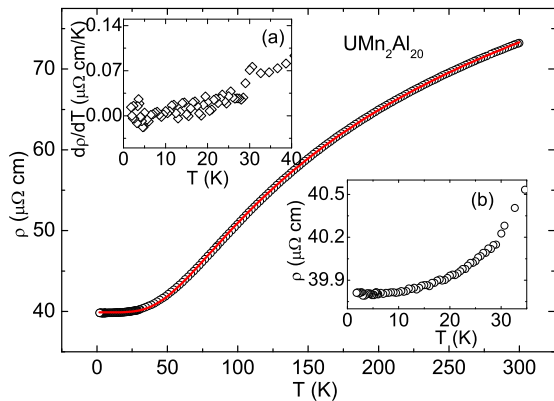


FIG. 4: (a) The resistivity $\rho(T)$ of $\text{UMn}_2\text{Al}_{20}$. The solid line is a fit to the parallel resistor model as described in the text. Inset (a) is the temperature differential curve and (b) is $\rho(T)$ below 35 K; no anomaly is observed at T_c .

that the magnetization measurements show clearly a ferromagnetic transition while no obvious anomaly associated with the transition is seen in the as-measured specific heat or the resistivity. Similar behavior is observed in the weak itinerant ferromagnetic compound ZrZn_2 ¹². The specific heat coefficient C_{mag}/T of $\text{UMn}_2\text{Al}_{20} = 0.3$ J/mole K² is large, suggesting that the ferromagnetic order occurs within a heavy Fermion state. Together with the moderately small moment of $0.90 \mu_B$, the similarity to ZrZn_2 suggests that this system may be a heavy Fermion itinerant ferromagnet. In this scenario, the reduced entropy and specific heat anomaly at T_c occurs because the entropy is already small due to the reduction of the moment by Kondo-like processes.

The Pauli paramagnetism seen for $\text{UV}_2\text{Al}_{20}$ and $\text{UMo}_2\text{Al}_{20}$ in Fig. 1(c) is also seen in $\text{LnT}_2\text{Al}_{20}$ (Ln=La, Ce and Eu, T=Ti, Mo and V)¹. This suggests that a tendency for the f electron to be non-magnetic is preferred in this structure. This lends further support to the scenario that the ground state of $\text{UMn}_2\text{Al}_{20}$ is essentially that of a weakly ferromagnetic itinerant heavy Fermion compound.

The small anomalies in $C(T)$ and $\rho(T)$ were also observed in Pr_3Tl ¹³ and Pr_3In ¹⁴, where induced ferromagnetic (antiferromagnetic) order occurs at 12 K^{13,14}. For these compounds, the $\text{Pr}^{3+} 4f^2$ ground multiplet is split by the crystal field such that the Γ_1 singlet is the ground state and the Γ_4 triplet is the lowest excited state. The Γ_1 ground state couples with Γ_4 triplet states through the intersite magnetic exchange interaction to induce a magnetic moment on the ground state^{13,14}. In mean field theories of the induced magnetic order, the ordering occurs within the singlet without loss of degeneracy, so that a very weak anomaly in the specific heat and resistivity is expected, reflecting the lack of a significant magnetic entropy change at the magnetic transition temperature. This has been taken as the explanation of the small anomalies in $C(T)$ and $\rho(T)$ in Pr_3Tl and Pr_3In .

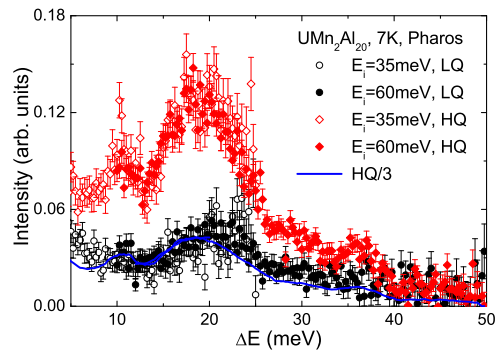


FIG. 5: The comparison of low Q and high Q inelastic neutron scattering spectra for $\text{UMn}_2\text{Al}_{20}$. Error bar in figure represents $\pm\sigma$. The data were collected on Pharos at two different incident energies. The solid line is the high Q data divided by a factor of 3.

In $\text{UMn}_2\text{Al}_{20}$, the uranium $5f$ electrons have the possibility of being in a $5f^2$ local moment configuration with a nonmagnetic $J=0$ ground state and a triplet excited state, which is the same $4f^2$ configuration as in the rare earth Pr^{3+} . Coupled with the absence of a specific heat $C(T)$ and electrical resistivity $\rho(T)$ anomaly at the transition temperature, this raises the possibility that this compound has a similar induced local moment behavior.

It has been proposed that the phase transition in induced moment systems is brought about by a softening of the crystal field excitation at the Q vector which corresponds to the magnetically ordered phase ($Q = 0$ for ferromagnetism; $Q = Q_N$ for antiferromagnetism). At a temperature much higher than the ordering temperature, well-defined non-dispersive crystal field excitations are expected but in the ordered state the singlet-triplet excitation would be dispersive¹⁵. These effects should be readily observable in neutron scattering spectra.

Therefore, in either the itinerant ferromagnetism case or the local moment induced ferromagnet case, there should be magnetic excitations in inelastic neutron scattering spectra corresponding either to the spin fluctuation (Kondo-like) scattering of the heavy fermion compound or to the crystal field excitations expected for a singlet-triplet induced moment system. Unfortunately, in the inelastic neutron scattering on a polycrystalline sample of $\text{UMn}_2\text{Al}_{20}$, there are no obvious magnetic excitations and all the peaks appear to be phonon contributions in the energy range of 5 meV to 50 meV (Fig. 5). Any magnetic excitations at these energies must overlap the phonon contribution. To estimate the phonon contribution, we utilize the observation⁵ that in the neutron scattering spectra for $\text{UCo}_2\text{Zn}_{20}$ and $\text{ThCo}_2\text{Zn}_{20}$, the phonon contribution at high Q is roughly 3 times larger than at low Q . Once the high Q spectra of $\text{UMn}_2\text{Al}_{20}$ is divided by a factor of 3, it is almost identical with the low Q spectra, suggesting that if there is magnetic scattering in this energy range, it is very weak.

In summary, we report a new ferromagnetic compound UMn_2Al_{20} for which a clear ferromagnetic transition is observed in the magnetic susceptibility but no strong anomaly was observed in the specific heat or resistivity. There appear to be two possible explanations for this behavior: moderately small moment itinerant ferromagnetism occurring in a heavy fermion state, or singlet-triplet induced local moment ferromagnetism. The inelastic neutron scattering spectra show no obvious magnetic excitations between 5 meV to 50 meV. More careful neutron scattering experiments to better determine the nonmagnetic scattering, and to explore the scattering at lower energies, are in order.

Acknowledgements Research at UC Irvine was sup-

ported by the U.S. Department of Energy, Office of Basic Energy Sciences, Division of Materials Sciences and Engineering under Award DE-FG02-03ER46036. Work at Los Alamos National Laboratory was performed under the auspices of the U.S. DOE/Office of Science. Work at ORNL was sponsored by the Laboratory Directed Research and Development Program of Oak Ridge National Laboratory, managed by UT-Battelle, LLC, for the U. S. Department of Energy. We acknowledge the support of the National Institute of Standards and Technology, U. S. Department of Commerce, in providing the neutron research facilities used in this work. Part of the work was supported by the National Science Foundation under grant no. DMR 0804032.

-
- ¹ Verena M. T. Thiede, W. Jeitschko, S. Niemann and T. Ebel, *J. Alloys and Compounds* **267**, 23 (1998).
- ² Kiichi Okuda, Satoru Noguchi, Yasuhiro Nakazawa and Masayasu Ishikawa, *J. Phys. Soc. Jpn.*, **58**, 4296 (1989).
- ³ I. Halevy, E. Sterer, M. Aizenshtein, G. Kimmel, D. Regev, E. Yahel, L. C. J. Pereira and A. P. Goncalves, *J. Alloys and Compounds* **319**, 19 (2001).
- ⁴ M. S. Torikachvili, S. Jia, E. D. Mun, S. T. Hannahs, R. C. Black, W. K. Neils, Dinesh Martien, S. L. Bud'ko and P. C. Canfield, *PNAS* **104**, 9960 (2007).
- ⁵ E. D. Bauer, C. Wang, V. R. Fanelli, J. M. Lawrence, E. A. Goremychkin, N. R. de Souza, F. Ronning, J. D. Thompson, A. V. Silhanek, V. Vildosola, A. M. Lobos, A. A. Aligia, S. Bobev and J. L. Sarrao, *Phys. Rev. B* **78**, 115120 (2008).
- ⁶ E. D. Bauer, A. D. Christianson, J. S. Gardner, V. A. Sidorov, J. D. Thompson, J. L. Sarrao, and M. F. Hundley *Phys. Rev. B* **74**, 155118 (2006).
- ⁷ J. S. Kim, G. R. Stewart and E. D. Bauer, *Phys. Rev. B* **78**, 035121 (2008).
- ⁸ C. H. Wang, A. D. Christianson, J. M. Lawrence, E. D. Bauer, E. A. Goremychkin, A. I. Kolesnikov, F. Trouw, F. Ronning, J. D. Thompson, M.D. Lumsden, N. Ni, E. D. Mun, S. Jia, P. C. Canfield, Y. Qiu, J. R. D. Copley, arXiv:1003.3484v1 (2010).
- ⁹ R. Hauser, E. Bauer, E. Gratz, Th. Holubar, A. Indinger, A. Lindbaum, W. Perthold, I. S. Dubenko and A.S. Markosyan, *Physica B* **206-207**, 17 (1995).
- ¹⁰ A. Arrott, *Phys. Rev.*, **108**, 1394 (1957).
- ¹¹ M. Calandra and O. Gunnarsson, *Phys Rev B* **66** (2002) 205105.
- ¹² E. A. Yelland, S. J. C. Yates, O. Taylor, A. Griffiths, S. M. Hayden and A. Carrington, *Phys. Rev. B* **72**, 184436 (2005); S. Ogawa, *Physica B*, **91**, 82 (1977).
- ¹³ K. Andres, E. Bucher, S. Darack and J. P. Maita *Phys. Rev. B*, **6**, 2716 (1972); P. Bossard, S. Bakanowaki, J. E. Crow, T. Mihalisin and W. J. L. Buyers, *J. Appl. Phys.* **50**, 1892 (1979).
- ¹⁴ A. D. Christianson, J. M. Lawrence, J. L. Zarestky, H. S. Suzuki, J. D. Thompson, M. F. Hundley, J. L. Sarrao, C. H. Booth, D. Antonio and A. L. Cornelius, *Phys. Rev. B* **72**, 024402 (2005); A. D. Christianson, J. M. Lawrence, K. C. Littrell, E. A. Goremychkin, A. I. Kolesnikov, J. D. Thompson and J. L. Sarrao, *J. Appl. Phys.* **101** 09D505 (2007).
- ¹⁵ R. J. Birgeneau, J. Als-Nielsen and E. Bucher *Phys. Rev. Lett.* **27**, 1530 (1971); W. J. L. Buyers, T. M. Holden and A. Perreault *Phys. Rev. B* **11**, 266 (1975); R. J. Birgeneau, J. Als-Nielsen and E. Bucher *Phys. Rev. B* **6** 2724 (1972).